scientific data

Check for updates

OPEN

DATA DESCRIPTOR

Landscape fire emissions from the 5th version of the Global Fire Emissions Database (GFED5)

Guido R. van der Werf[1] ✉, James T. Randerson[2], Dave van Wees[3], Yang Chen[2], Louis Giglio[4], Joanne Hall[4], Vernooij Roland[1], Mingquan Mu[2], Samiha Binte Shahid[5], Kelley C. Barsanti[6], Robert Yokelson[7] & Douglas C. Morton[8]

Landscape fires are a major source of greenhouse gases and other atmospheric constituents. Most global inventories of landscape fire emissions have converged at around 2 petagram of carbon (Pg C) y^{-1} since satellite information on burned areas became available in the early 2000s. These emission estimates are known to be uncertain, and studies using satellite measurements of column carbon monoxide or aerosol optical depth found that emissions from regional fire complexes often exceed estimates from global inventories. Here we describe the development of the fifth version of the Global Fire Emissions Database (GFED5), which incorporates new information on burned area, improved modelling of fuel loadings, and new emission factors. GFED5 total global landscape fire carbon emissions are 3.4 Pg C y^{-1} (2002–2022 average) and closer in line with atmospheric constraints for several key fire events than its predecessor GFED4s. This new landscape fire emission dataset advances and extends the record needed to improve dynamic fire models and interpret the burden, impacts, growth rates, and variability of atmospheric trace gases and aerosols.

Background & Summary

Fire has played a crucial role in shaping the Earth's ecosystems for at least 420 million years[1]. The study of global fire dynamics and their impacts has recently intensified, spurred by new satellite observations and the growing effects of changing fire regimes driven by climate change, land use change, and evolving forest management practices[2,3]. Although the role of fire in governing atmospheric budgets of gases and aerosols, as well as in modifying cloud patterns, has been described in the literature since at least the late 19th century[4], the first quantitative assessments of biomass burning emissions were developed in the late 1970s[5,6]. These early studies estimated that total fire carbon emissions were between 2 and 4 Pg C y^{-1}, based on aggregating biome-level fire return times and biomass loadings, as well as combining population density and per-person land requirements associated with shifting cultivation and deforestation. Later refinements followed a similar book-keeping approach[7], and were motivated by a need to further improve understanding of fire impacts on atmospheric composition.

The first global gridded emissions estimates became available in the mid-2000s, leveraging advances in satellite-derived burned area mapping at continental scales and the development of biogeochemical models that tracked carbon flows, and enabled quantitative estimates of fuel consumption (the amount of biomass combusted per unit burned area). Estimates from these early geospatial models varied widely[8,9], from 1.7 to 3.5 Pg C y^{-1}. Variation among different model approaches stemmed mainly from large uncertainties in burned area and fuel consumption. However, some of the differences were also due to the analysis of different time intervals and high levels of interannual variability in emissions. Over time, contemporary global burned area assessments have increased from about 200 million hectares (Mha) y^{-1} (ref. [10]) to well over 400 Mha y^{-1} for the latest burned area assessments using Moderate Resolution Imaging Spectroradiometer (MODIS) imagery[11,12]. For more than

[1]Meteorology and Air Quality Group, Wageningen University & Research, Wageningen, the Netherlands. [2]Department of Earth System Science, University of California, Irvine, CA, USA. [3]BeZero Carbon, London, UK. [4]Department of Geographical Sciences, University of Maryland, College Park, MD, USA. [5]Department of Chemical and Environmental Engineering, University of California-Riverside, Riverside, CA, USA. [6]Atmospheric Chemistry Observations and Modeling Laboratory, NSF National Center for Atmospheric Research, Boulder, CO, USA. [7]Department of Chemistry and Biochemistry, University of Montana, Missoula, MT, USA. [8]Biospheric Sciences Laboratory, NASA Goddard Space Flight Center, Greenbelt, MD, USA. ✉e-mail: guido.vanderwerf@wur.nl

two decades, MODIS-derived surface reflectance products have served as the primary source used to assess burned area trends and variability across biomes and continents.

In parallel to the increasingly larger burned area estimates, fuel consumption estimates have decreased over time, partly offsetting the influence of changing burned area assessments in global inventories. Consecutive versions of the Global Fire Emissions Database (GFED) had multi-year average global carbon emissions slightly above 2 Pg C y^{-1} (refs. [13,14]). This 2 Pg C y^{-1} estimate has been used in the Global Carbon Project's budgets for carbon dioxide[15], methane[16], and nitrous oxide[17]. It has also helped to constrain fire models in the Fire Model Intercomparison Project[18], contributed to the development of the Global Fire Assimilation System (GFAS[19]), served as a data source for IPCC reports[20], and been used to quantify fire effects on atmospheric composition and radiative forcing[21–24].

For over a decade, however, it has been recognized that burned area estimates may still be conservative as a consequence of limits in our ability to detect small fires[25]. This suggests that the widely used 2 Pg C y^{-1} estimate of global fire emissions may also be an underestimate. Most global burned area products have typically relied on 500-m[11] or 250-m[12] surface reflectance data, but in many biomes, a considerable number of fires are smaller than an individual pixel and therefore often go undetected. These so-called small fires can be detected using active fire data or higher spatial resolution burned area. The initial estimates of additional small-fire burned area boosted the global burned area by approximately 35% (refs. [25,26]). However, subsequent studies indicated that these small fires are even more prevalent than initially assumed[27,28]. In Africa, for example, the use of 20 m Sentinel-2 surface reflectance data for continent-wide mapping yields burned area estimates that are approximately double the MODIS 500-m estimates[29].

In agricultural areas, a careful evaluation of sub-pixel burning yields an even larger boost in burned area; a new study[30] estimated that between 2003 and 2020, the average annual global cropland burned area was 81 Mha y^{-1}. This is more than 150% higher than the 32 Mha y^{-1} estimated by the MODIS 500-m MCD64A1 dataset[11]. Recent research that integrates active fire and higher-resolution reference burned area maps with the 500-m MODIS product indicates that on a global scale, contemporary total burned area is about 770 Mha y^{-1} for 2001–2020 (ref. [28]). This estimate, which accounts for commission and omission errors in the 500-m MODIS burned area time series (including a better representation of small fires), yields a 93% increase in the global area burned compared to the MODIS MCD64A1 dataset, with the importance of small fires varying considerably within and across different biomes.

The gradual improvement in burned area algorithms, combined with step-changes in satellite spatial resolution, has led to more accurate estimates of burned area. At the same time, new sensors, algorithms, and observations have helped to improve estimates of fuel consumption. For example, data from spaceborne lidar are beneficial for assessing changes in aboveground tree biomass resulting from fire[31]. In addition, the more challenging task of constraining surface fuel dynamics can now be partly addressed on regional scales using a combination of satellite[32,33] and lidar[34] observations. The improved spatial resolution and geolocation accuracy of higher resolution burned area products enable better alignment of burned area with land cover, thereby facilitating more accurate characterization of fuel loads. However, despite the growing use of satellite data in constraining several aspects of fuel consumption, modeling is still required, for example, for surface detrital pools, which are often the main component of total fuel consumption. New field measurements of fuel consumption are crucial for constraining fuel models. Over the past decade, several large field campaigns have included fuel consumption as a key measurement objective. These efforts include NASA's Arctic-Boreal Vulnerability Experiment (ABOVE[35]) in boreal North America, as well as extensive fuel consumption studies in savanna regions, particularly in southern Africa[33,36].

Emission factors (in units of grams of emitted chemical species per kilogram of dry matter burned) are often used in a final step to convert fire carbon emissions into emissions of trace gases and aerosols. Over the past decade, improvements in measurement capabilities and major field campaigns have considerably reduced uncertainties within this component of inventories. Campaigns such as the Fire Influence on Regional to Global Environments and Air Quality (FIREX-AQ[37]) have yielded more accurate information on many species. At the same time, field measurements in key biomes have enabled a better understanding of under-sampled areas, including, for example, peat fires in Indonesia[38,39]. Within-biome variability is becoming better understood as well, both due to employing satellite-based estimates of trace gases[40] and by analyzing the causes of measured *in-situ* variability, for example, within the global savannas[41]. In addition, tower-based measurements of emitted gases, in combination with atmospheric modeling, enable an analysis of larger fire complexes for a full fire season and have led to an improved characterization of CO and CH_4 emission factors in boreal forests of North America[42]. Many of these studies are integrated in the recently developed Next-generation Emissions InVentory expansion of Akagi *et al.* (NEIVA) fire emission factor synthesis[43], building on previous emission factor compilations[44,45] but employing a more systematic and flexible approach to compute biome-level average emission factors.

Here we describe how we used these developments to build the fifth version of GFED (GFED5). We combined new burned area estimates[28,30] with a fuel consumption model constrained by observations[46] to estimate fire carbon losses for GFED5. Converting fire carbon losses to emissions of trace gases and aerosols was primarily based on NEIVA[43], augmented by several new studies that aimed to understand the emission factors at landscape-scales[41,42].

Methods

Overview. Since its inception in 2004, emission estimates from GFED have been computed by multiplying burned areas, fuel loads, combustion completeness factors, and emission factors within a biogeochemical modeling framework. In GFED5, each of those parameters has undergone substantial revision compared to the previous GFED4(s) dataset, each of which is further described below. An overview of the methodology is shown

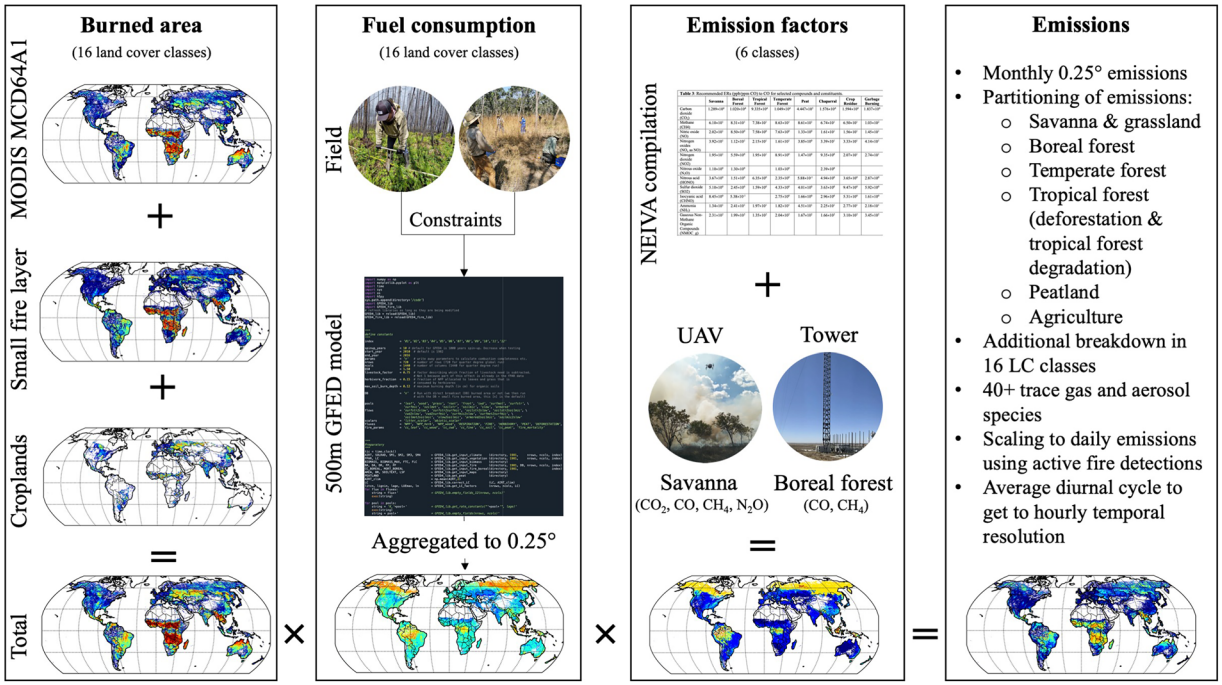

Fig. 1 Overview of the approach used to construct GFED5. Fire emissions are derived from multiplying burned area, fuel consumption (fuel loads × combustion completeness), and emission factors for each time step and 0.25° grid cell.

in Fig. 1. We focus on the 2002–2022 period when high-quality data products from MODIS are available, and then describe in a subsequent step how we extend the emissions time series back to 1997, using other satellite data records. A separate paper will discuss extending the time series forward using Visible Infrared Imaging Radiometer Suite (VIIRS) active fire detections.

The core GFED5 spatial resolution is 0.25°, and the temporal resolution is monthly. This resolution enables improved statistical estimation of cropland[30] and small fire burned area layers[28]. Within each 0.25° grid cell, burned area is distributed over 16 land cover classes and aligned with the fuel consumption for the same land cover class each month. The fuel loads and consumption are derived using a light-use efficiency model as in previous versions of GFED[13,26]. Modelled biomass and derived fuel loads are computed for each grid cell and each month as the difference between biomass in the previous month for that grid cell, input of net primary production (NPP) based on the light-use efficiency model, and losses from respiration and fire. The key difference with previous GFED versions is that we now run this model at a 500-m spatial resolution[46], which we subsequently aggregate here to 0.25°. The 500-m model employs a refined multi-step calibration procedure, an enhanced method for calculating tree mortality using forest loss data, and parameterizations for emissions from belowground burning. For GFED5, fuel consumption within each 0.25° grid cell is calculated for each land cover type, weighted by the 500-m MODIS MCD64A1 burned area. Carbon emissions in GFED5 are derived by multiplying the GFED5 burned area and fuel consumption for the land cover types present within each 0.25° grid cell, and are then aggregated into 6 fire categories for which we have emission factor information. Finally, these monthly emission estimates can be converted to higher temporal resolution using active fire observations from multiple satellite sensors. These steps are explained in more detail below.

Burned area. We used the GFED5 burned area dataset[28], which followed a similar approach as our earlier work[25] in the sense that the MODIS-mapped burned area[11] is augmented with MODIS active fire detections to estimate omission and commission errors in the MODIS-mapped burned area product. The main difference between our new[28] and previous work[25] is that medium-resolution burned area datasets (i.e., Landsat or Sentinel-2-derived reference maps) for selected regions and time periods are now used to constrain correction factors to account for omission and commission errors. Omission errors are mostly small fires; commission errors are often related to unburned patches or "islands" within larger burns.

We extended the GFED5 burned area dataset[28] through 2022 and made minor adjustments to the commission and omission scale factors for several temperate forest regions. This burned area time series will be referred to as version 5.1. This version number will also be used for the derived emissions, but is referred to here simply as GFED5. Specifically, the commission and omission scaling coefficients in two temperate classes, temperate forest and temperate mosaic, were updated for Australia (AUST, see Fig. 2) using Sentinel-2-based reference data (2016–2021) from the Fire Extent and Severity Mapping (FESM) program (https://datasets.seed.nsw.gov.au/dataset/fire-extent-and-severity-mapping-fesm). The use of these reference data improved our ability to capture the magnitude and interannual variability of burned area in forest ecosystems in this region.

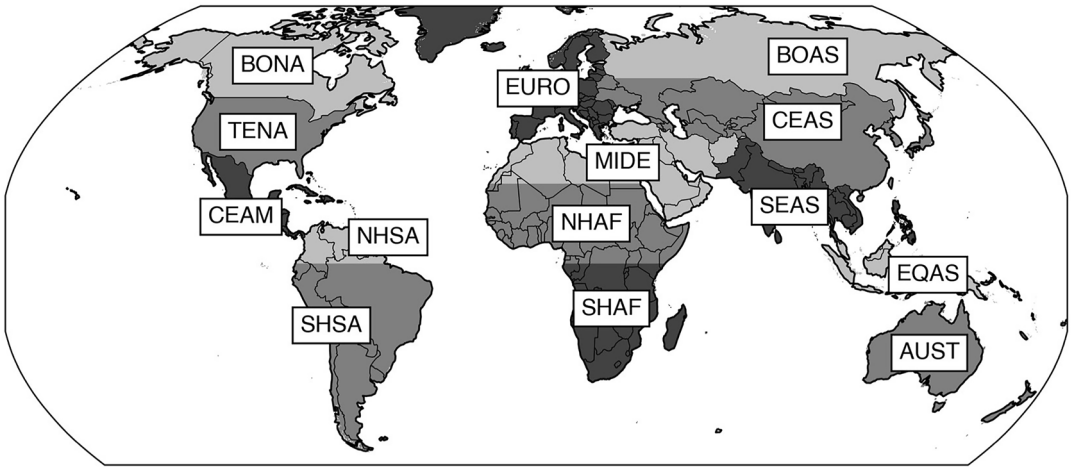

BONA	Boreal North America	NHAF	Northern Hemisphere Africa
TENA	Temperate North America	SHAF	Southern Hemisphere Africa
CEAM	Central America	BOAS	Boreal Asia
NHSA	Northern Hemisphere South America	CEAS	Central Asia
SHSA	Southern Hemisphere South America	SEAS	Southeast Asia
EURO	Europe	EQAS	Equatorial Asia
MIDE	Middle East	AUST	Australia and New Zealand

Fig. 2 A map of the 14 continental-scale regions used to aggregate and report fire statistics in this study.

Similarly, we updated the commission scaling coefficients for temperate forest/shrub biomes in the temperate North America region (TENA, see Fig. 2) using Landsat-derived burned perimeters from the Monitoring Trends in Burn Severity program (MTBS, https://www.mtbs.gov/) for the period 2011–2020. This commission error adjustment focused only on MODIS-mapped burns and MTBS polygons within those burn scars. We did not adjust the omission error using the MTBS data, given its potential to encapsulate some unburned patches within the fire perimeter polygon[47].

For agricultural areas, we used the global cropland area burned (GloCAB) dataset[30]. The dataset originally covered the 2003–2020 period and was recently extended to include 2021 and 2022. Because agricultural burns are typically small, GloCAB relies on a large set of high-resolution reference burned-area scenes derived from Sentinel-2 (20 m), Landsat-8 (30 m), and PlanetScope (3 m) imagery. These reference scenes encompass a wide range of crop types across five continents, with particular emphasis on Ukraine, Russia, and the United States. Extrapolation in time and space is based on relations between these reference scenes and MODIS active fire detections (MCD14ML[48]) using global maps of crop type. To estimate cropland burned area for 2001–2002, we applied a scaling approach similar to that used for other GFED5 burned area classes[28]. This method uses Terra MODIS active fire detections within the cropland pixels and applies a region-specific calibration factor derived from the GloCAB dataset for 2003–2020.

Total global burned area, including agricultural fires (2002–2022 average), was 759 Mha y^{-1} (Table 1), 88% higher than MCD64A1 Collection 6.1 and 61% higher than GFED4s for the 2002–2016 overlapping period. Relatively speaking, increases in agricultural burning were even larger; GloCAB has 80 Mha (2003–2022 average, marginally lower than the earlier mentioned 81 Mha for 2002–2020), over 150% more burned area in croplands than MCD64A1. The difference between GFED5.1 and GFED5 burned area is small (1 Mha y^{-1}, averaged over 2002–2022) compared to the global total burned area. However, for the temperate land cover classes, this still represented a 5% increase in burned area.

As in GFED4, our burned area data has a spatial resolution of 0.25° to ensure statistical robustness when assessing commission and omission errors. A higher spatial resolution would jeopardize the soundness of relationships between out-of-burn active fires and the moderate resolution reference burned area used to construct omission and commission scalars. However, sub-grid cell information on the contribution of each land cover type to the total grid cell burned area is now tracked and used in the conversion of burned area to fire carbon emissions.

Fuel consumption. Fuel consumption (fuel load × combustion completeness) in GFED has always been based on the Carnegie-Ames-Stanford-Approach (CASA) biogeochemical model[49]. In this model, fuel loads are calculated dynamically as the difference between inputs from satellite-derived estimates of NPP, allocation of NPP into herbaceous and woody vegetation pools, and losses from living and detrital pools estimated using climate and fire observations[14,26]. In a previous study[46], which will be referred to as the donor study, we built a 500-m resolution version of this model, focusing primarily on the processes that are relevant for the build-up of aboveground fuels, while simplifying, for example, belowground processes.

Region	Savanna and Grassland	Boreal forest	Temperate forest	Tropical forest	Peatland	Agriculture	All
BONA	0.2	2.7	0.1		0.0	1.3	4.2
TENA	3.2		0.4		0.0	3.0	6.7
CEAM	9.1		0.1	0.7	0.1	2.5	12.5
NHSA	8.2			0.3	0.2	0.4	9.2
SHSA	44.1		0.2	4.0	0.7	4.2	53.2
EURO	1.3	0.1	0.1			2.6	4.1
MIDE	0.6		0.0		0.0	2.6	3.2
NHAF	215.0			1.9	0.4	19.4	236.6
SHAF	236.1		0.1	2.1	0.7	2.4	241.5
BOAS	11.4	12.2	1.5		0.1	6.2	31.3
CEAS	19.7	0.5	0.6	0.1	0.1	19.6	40.6
SEAS	42.4		0.1	2.7	0.3	13.5	59.0
EQAS	1.9			0.5	0.5	0.7	3.7
AUST	49.7		1.0	0.0	0.0	1.8	52.5
All	642.9	15.5	4.1	12.4	3.3	80.3	758.5

Table 1. Mean annual burned area in Mha y^{-1} averaged over 2002–2022 for different regions and fire categories. Empty cells have, on average, less than 0.1 Tg C y^{-1} emissions during 2002–2022 (Table 5). Region abbreviations are explained in Fig. 2, and the various fire categories are described in Table 2.

In the 500-m fuels model, NPP is calculated using the product of downwelling solar radiation received at the surface from ERA5-land reanalysis[50], the fraction of photosynthetically active radiation absorbed by vegetation (fPAR) from MODIS[51], and scalars that represent temperature or water stress, also based on ERA-5. NPP is allocated to different pools (i.e., leaf, stem, root) using pre-defined ratios between above- and belowground pools and fractional tree cover information[52]. Land cover-specific turnover rates govern when carbon is transferred from live to dead pools. These dead pools also respire based on turnover rates, but are mediated by scalars representing moisture and temperature limits on decomposition rates. Tree mortality is derived from Global Forest Change (GFC) forest loss data[53] and its overlap with burned area and active fire detections. The tree mortality information is used to calculate both forest loss without fire, such as logging (which is not used for GFED5 fire emissions, although its impact on fuel loads is accounted for), and fire-related forest loss, such as stand-replacing fire, shifting agriculture, and commodity-driven deforestation.

When a 500 m grid cell burns, a fraction of each pool can be combusted, depending on the tree mortality and a combustion completeness scalar. Consumption of belowground carbon (e.g., in peatlands) is modelled using pre-defined carbon density for surface litter and organic duff layers, a set maximum burning depth (which varies regionally), and a scalar based on soil moisture that governs the actual depth of burning. A more detailed description can be found in Van Wees *et al.*[46].

The 500-m model allowed us to constrain fuel consumption better using fuel consumption measurements[54,55] given that the increased spatial resolution led to better alignment of the model with actual measurements[46]. This optimization process was primarily based on tuning turnover rates for various fire-relevant biomass pools. In its second release, the model was extended to 2022, and all input datasets were updated to their most recent versions (https://doi.org/10.5281/zenodo.12670427).

Aggregation of fuel consumption to the 0.25° GFED5 grid was performed for each of the burned area classes listed in Table 2, using the sub-grid cell burned area derived from the number of MCD64A1 burned area pixels within each class. If in a given month and 0.25° grid cell no fuel consumption was available from the 500-m model for a specific class (for example, because GFED5 burned area only stemmed from active fire detections and not from mapped MCD64A1 burned area), we used a value derived from nearest neighbor interpolation. The 500-m donor study[46] included burned area outside of mapped MCD64A1 burned area that overlapped with areas of forest loss. These were excluded here to avoid double-counting with the small fire burned area layer, which is also derived from active fire detections outside mapped burned area.

For GFED5, we made several modifications to the fuel consumption estimates derived from Van Wees *et al.*[46]. The first update is related to the difference in spatial resolution between GFED5 (0.25°) and the 500-m fuel consumption dataset. The addition of small fires in GFED5 (not included in the 500-m dataset) led to a substantial number of 0.25° grid cells with relatively high fractional tree cover having frequent fires. In the 500-m dataset, we could distinguish between stand-replacing fires and other categories based on overlapping burned area and forest loss[53]. This is not possible when using the GFED5 burned area because small fires are based on active fire detections scaled to burned area in a statistical framework. To overcome this issue and prevent the unrealistic combination of frequent burning and stand-replacing fires for an extended period, we assumed that the total forest burned area during 2002–2022 could not exceed the total forest area within each grid cell. For this calculation, forest area was based on the 2001–2003 average fraction of tree cover (FTC) from the MOD44B Version 6 Vegetation Continuous Fields (VCF) dataset[52]. The remainder of the burned area was considered ground fire that generated fuel consumption only from grass and fine litter pools. This adjustment primarily impacted the southern edge of the boreal region, Southeast Asia, and woodlands bordering the tropical forest region in Africa.

Second, the fuel consumption for agriculture was scaled with a factor of 0.63 so that the average fuel consumption from the model matched the average fuel consumption from agricultural field measurements. It is

Burned area class	Reclassification for carbon emissions modeling	Fuel consumption correction	Emission factor class
Tundra	—	—	Boreal forest
Sparse boreal forest	—	FTC correction[4]	Boreal forest
Boreal forest	—	FTC correction[4]	Boreal forest
Temperate grassland	—	—	Savanna & grassland
Temperate shrubland	—	—	Savanna & grassland
Temperate mosaic	—	—	Savanna & grassland
Temperate forest	—	—	Temperate forest
Tropical grassland	—	—	Savanna & grassland
Tropical shrubland	—	—	Savanna & grassland
Open savanna	—	—	Savanna & grassland
Woody savanna	—	—	Savanna & grassland
Tropical forest	When in Evergreen Broadleaf forest → Tropical forest	FTC correction[4]	Tropical forest
	Remainder in woody savanna	FTC correction[4]	Savanna & grassland
Other[1]	—	—	Savanna & grassland
Cropland[2]	—	Fuel consumption scaled with a factor of 0.63 to match field observations	Cropland
Peatland[3]	—	—	Peatland
Deforestation	When in In Evergreen Broadleaf forest → Deforestation	—	Tropical forest
	When in Deciduous Needleleaf or Deciduous Broadleaf forest → Temperate forest	—	Temperate forest
	Remainder in woody savanna	—	Savanna & grassland

Table 2. Mapping approach for GFED5 burned area, carbon emissions modeling, and application of emission factors to estimate fire-emitted trace gases, based primarily on annually varying MODIS MCD12Q1 land cover type using the IGBP scheme[80]. [1]Consisting of classes water, urban, snow and ice, and barren. [2]Combination of classes cropland and cropland/natural vegetation mosaic, and only taking grass and fine litter carbon pools into account to compute fuel consumption. [3]Includes aboveground vegetation. [4]Total forest burned area over 2002–2022 could not exceed the fractional tree cover (FTC, average of 2001–2003) in forests.

important to note that the number of field sites to constrain the model for agricultural fuel consumption is very limited. In total, nine measurement locations were available (one in Spain, one in Thailand, two in the US, and five in China). Further, the sites in China were all located in the same 0.25° grid cell. While more field data on agricultural fuel consumption is necessary to quantify and reduce uncertainties, future efforts to better constrain agricultural fire emissions and their spatial and temporal variability could also use maps of crop type, reported harvest rates, and residue-to-harvest ratios. For now, we consider cropland burning emissions one of the most uncertain categories. Burned area in the 'other class' (consisting of water, urban, snow and ice, and barren), which had no fuel consumption in the 500-m donor database[46], received the average fuel consumption from other land cover classes (area-weighted) for that same grid cell.

We re-classified the vegetation or burned area classes to the 16 land cover classes listed in Table 2 for the estimation of grid-cell level fuel consumption and subsequently to compute carbon emissions. The main difference between the classes tropical forest and deforestation is the geographic domain and the approach for calculating fuel consumption. The GFED5 deforestation burned area is a subset of the tropical forest biome, separated by fraction tree cover (>20%) and fire persistence based on repeated MODIS active fire detections (mean fire persistence >1.5), see Chen *et al.*[28]. The corresponding fuel consumption in this class is higher than tropical forest fuel consumption due to higher combustion completeness, to represent commodity-driven deforestation[46]. Peatland fuel consumption included both above- and belowground fuels, with the depth of burning in belowground fuels being governed by soil moisture conditions[46]. As in the 500-m donor dataset[46], the burn depth in South American peatlands was halved compared to Indonesian peatlands to reflect lower levels of drainage. The burn depth for peatlands in Africa and in the extratropics was multiplied by 0.1 to reflect a weaker anthropogenic influence on the water table in these areas.

In a separate step, the emissions from the 16 fire classes were aggregated into six aggregated classes to enable the application of emission factor information (see below). This final step did not affect fuel consumption from the upstream carbon emissions modeling step; therefore, we will report emissions for these six aggregated classes here. Figure 3 and Table 3 describe the distribution of fuel consumption estimates by vegetation type and region, while Fig. 4b illustrates the spatial pattern at the grid cell level. The global average fuel consumption was 443 g C per m^2 of burned area over the 2002–2022 time period. For the 2002–2016 period, when GFED4s had burned area available, GFED5 fuel consumption is 4% lower than GFED4s (433 versus 451 g C m^{-2} burned).

Carbon emissions. Global fire carbon emissions averaged over 2002 to 2022 were 3.4 Pg C y^{-1}, with the African continent accounting for just over half of these emissions (Tables 4, 5). The spatial map (Fig. 4c) resembles the burned area distribution (Fig. 4a), but is weighted towards regions with higher fuel loads and levels of combustion completeness. Interannual variability in emissions is larger than in the burned area dataset, especially in regions where forests and peatlands are key drivers of fire patterns (e.g., boreal North America, boreal Asia, and equatorial Asia; see Table 4).

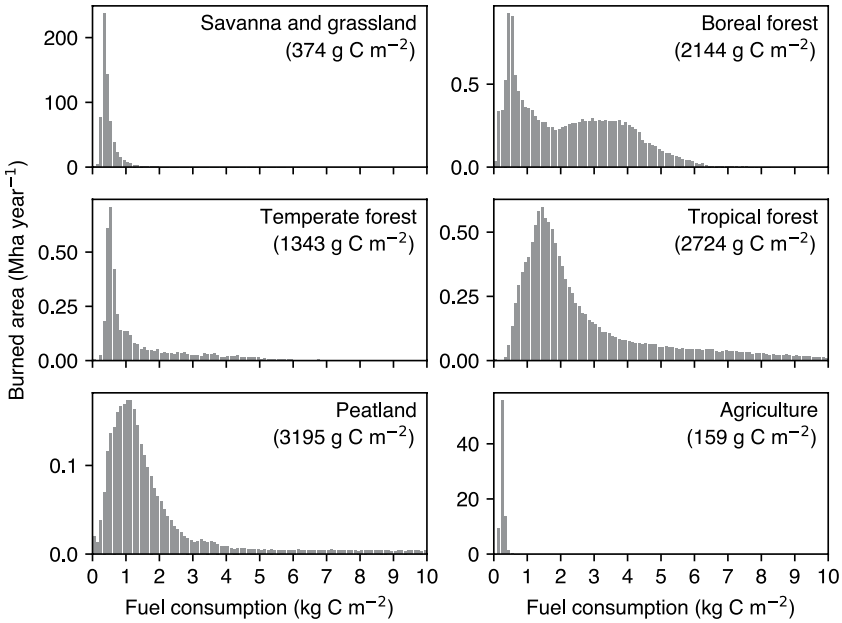

Fig. 3 Fuel consumption distribution (bins of 100 g C m^{-2} burned) for our six aggregated fire categories, averaged over 2002–2022. The tropical forest class includes deforestation and degradation fires. The numbers indicate the burned area weighted average fuel consumption for each fire category.

Region	Savanna and Grassland	Boreal forest	Temperate forest	Tropical forest	Peatland	Agriculture	All
BONA	1052	3116	1558		2452	195	2110
TENA	488		1767		1010	199	444
CEAM	678		1999	2449	1464	225	706
NHSA	297			2271	1317	124	385
SHSA	496		2078	4246	2068	166	775
EURO	541	619	1233			210	353
MIDE	289		1737		1335	176	215
NHAF	304			1748	1273	149	304
SHAF	389		1675	1831	1260	191	403
BOAS	264	2009	493		1934	152	932
CEAS	190	646	1004	1533	705	163	197
SEAS	659		930	1773	1515	118	592
EQAS	808			4226	11991	162	2877
AUST	282		2377	1676	1655	230	322
All	374	2144	1343	2724	3195	159	443

Table 3. Mean fuel consumption (g C m^{-2} burned) for the 2002–2022 period for different regions and fire categories. Empty cells have, on average, less than 0.1 Tg C y^{-1} emissions during 2002–2022 (Table 5). Region abbreviations are explained in Fig. 2, and the various fire categories are described in Table 2.

The magnitude of emissions in most regions is considerably higher in GFED5 than in GFED4s. However, in general, they show similar interannual variability (Fig. 5). The largest relative difference was found in Southeast Asia (+223%) and in the Middle East (+222%). Given its low magnitude, the Middle East remains a low fire region, but according to GFED5, Southeast Asia is now the fourth-highest fire region among our basis regions, ranking behind southern and northern hemisphere Africa, and southern hemisphere South America. Only equatorial Asia had a decline in emissions compared to GFED5 (−10%), mostly from lower emissions in high fire years due to recalibrated tropical peat fire emissions[46].

Emission factors. To convert fire carbon losses to emissions of trace gases and aerosols, we used the NEIVA database[43] version 1.1 with several modifications. NEIVA builds on earlier emission factor compilations[44,45] but includes the results from new studies carried out since then, including laboratory studies. Emission factors are the arithmetic means of all available measurements. In GFED5, we aggregated our 16 land cover classes into the six fire categories relevant for landscape fires in NEIVA (Table 2). The variability in emission factors between studies

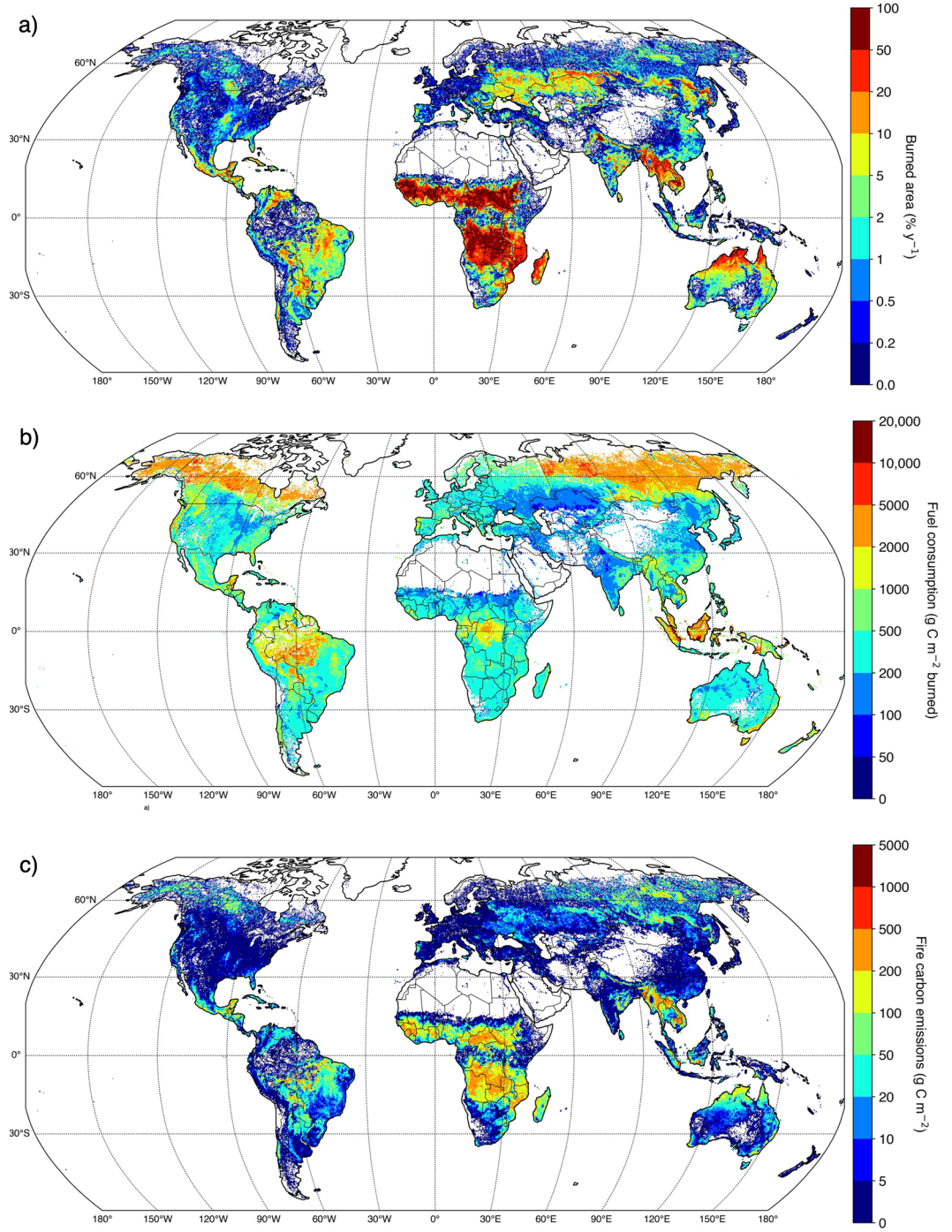

Fig. 4 Mean annual burned area (**a**), fuel consumption (**b**), and fire carbon emissions (**c**) from GFED5 on its native 0.25° grid, averaged over 2002–2022.

is often considerable, frequently exceeding the mean. Emission factors are given in grams of emitted species per kg of dry matter (DM) burned, and we used the CO_2, CO, and CH_4 emission factors together to compute the dry matter carbon content (Table 6).

In GFED5, we replaced the NEIVA emission factors of CO_2, CO, CH_4, and N_2O in savannas and grasslands with dynamic emission factors[41]. The substituted values were based on a set of 129 fires sampled mostly using an unmanned aerial vehicle (UAV) on three different continents, over a rainfall gradient, and at various times during the fire season. This set was complemented with measurements from 85 other savanna fires from the literature and used to train a random forest model that described the spatial (0.25°) and temporal (daily) variability in the emission factors. Key drivers for the observed variability were vapor pressure deficit (VPD), fractional tree cover, and the fire weather index (FWI). Weighted biome-averaged CO and CH_4 emission factors were close to previous compilations as used in GFED4s but lower than in NEIVA. The main difference with GFED4s was the

Region	Burned area in Mha y^{-1} (share (%))	Carbon emissions in Tg C y^{-1} (share (%))	Standard deviation (%)	Minimum in Tg C y^{-1} (year)	Maximum in Tg C y^{-1} (year)
BONA	4.2 (0.6)	88.9 (2.6)	52	13 (2020)	213 (2004)
TENA	6.7 (0.9)	29.8 (0.9)	34	17 (2019)	61 (2020)
CEAM	12.5 (1.7)	88.5 (2.6)	22	55 (2014)	131 (2011)
NHSA	9.2 (1.2)	35.3 (1.0)	32	18 (2011)	59 (2016)
SHSA	53.2 (7.0)	412.0 (12.2)	29	238 (2013)	655 (2005)
EURO	4.0 (0.5)	14.2 (0.4)	31	9 (2014)	26 (2017)
MIDE	3.1 (0.4)	6.6 (0.2)	23	4 (2022)	9 (2009)
NHAF	236.7 (31.2)	719.3 (21.4)	9	602 (2019)	901 (2016)
SHAF	241.5 (31.8)	973.6 (28.9)	5	862 (2006)	1060 (2013)
BOAS	31.6 (4.2)	294.8 (8.8)	42	126 (2004)	568 (2012)
TEAS	40.4 (5.3)	79.4 (2.4)	28	45 (2021)	125 (2008)
SEAS	59.2 (7.8)	350.2 (10.4)	19	200 (2002)	450 (2010)
EQAS	3.5 (0.5)	101.5 (3.0)	91	9 (2022)	353 (2015)
AUST	52.6 (6.9)	169.7 (5.0)	29	88 (2010)	286 (2019)
All	758.5 (100.0)	3363.8 (100.0)	6	2881 (2022)	3670 (2015)

Table 4. Mean annual burned area and emissions by region, and metrics to quantify interannual variability, including standard deviation and years of minimum and maximum emissions. Region abbreviations are explained in Fig. 2.

Region	Savanna and Grassland	Boreal forest	Temperate forest	Tropical forest	Peatland	Agriculture	All
BONA	1.6	82.9	1.2		0.7	2.5	88.9
TENA	15.6		7.7		0.4	6.0	29.8
CEAM	61.6		2.7	17.2	1.3	5.7	88.5
NHSA	24.5			7.5	2.9	0.5	35.3
SHSA	218.8		3.3	168.1	14.7	7.0	412.0
EURO	6.7	0.7	1.4			5.4	14.2
MIDE	1.5		0.4		0.4	4.4	6.6
NHAF	652.7			32.5	5.1	29.1	719.3
SHAF	919.3		1.2	39.3	9.2	4.6	973.6
BOAS	30.8	245.5	7.4		1.8	9.3	294.8
CEAS	37.0	2.9	5.4	1.1	0.7	32.3	79.4
SEAS	280.1		0.5	49.0	4.6	15.9	350.2
EQAS	14.6			22.5	63.3	1.1	101.5
AUST	140.3		24.1	0.5	0.7	4.1	169.7
All	2405.1	332.3	55.1	337.7	105.7	128.0	3363.8

Table 5. Mean annual fire carbon emissions in Tg C y^{-1}, averaged over 2002–2022 for different regions and fire categories. Empty cells have, on average, less than 0.1 Tg C y^{-1} emissions during 2002–2022. Region abbreviations are explained in Fig. 2, and the various fire categories are described in Table 2.

lower weighted biome-averaged N_2O emission factor (0.15 in GFED5 versus 0.20 in GFED4s). For other species in savannas and grasslands, the NEIVA averages were used. However, in the savanna and grassland category, we excluded two studies to compute the average as they were not representative of the larger tropical savanna biome, being either from prescribed fires under wet conditions in temperate grasslands[56] or from fires in the very early dry season in the Australian savanna, when the vegetation was still moist[57].

A second adjustment we made was to the CO and CH_4 emission factors in boreal forests. NEIVA includes laboratory, field, and airplane measurements, but does not incorporate integrative approaches such as surface tower observations or satellite-based estimates to obtain biome-level emission factors. One such tower study[42] was carried out in Alaska during the 2015 high fire year, using continuous measurements of CO_2, CO, and CH_4 from the Carbon in Arctic Reservoirs Vulnerability Experiment (CRV) tower in Fox, Alaska. In combination with transport modelling, 34 individual fires could be sampled, yielding higher values for CO (127 g CO per kg dry matter burned from the tower versus 100 from NEIVA) and CH_4 (5.3 g CH_4 per kg dry matter burned from the tower versus 4.8 from NEIVA). We averaged the tower and NEIVA values and noted that the boreal forest emission factors are primarily representative of North American boreal forests, which likely have an overall higher MCE than forests in boreal Asia[40,42]. Finally, for some fire categories, not all species were represented in the NEIVA database. Missing values were filled in using data other fire categories with the strongest similarity, see footnotes in Table 6. The missing OC and TPC emission factors from boreal forests were derived in a

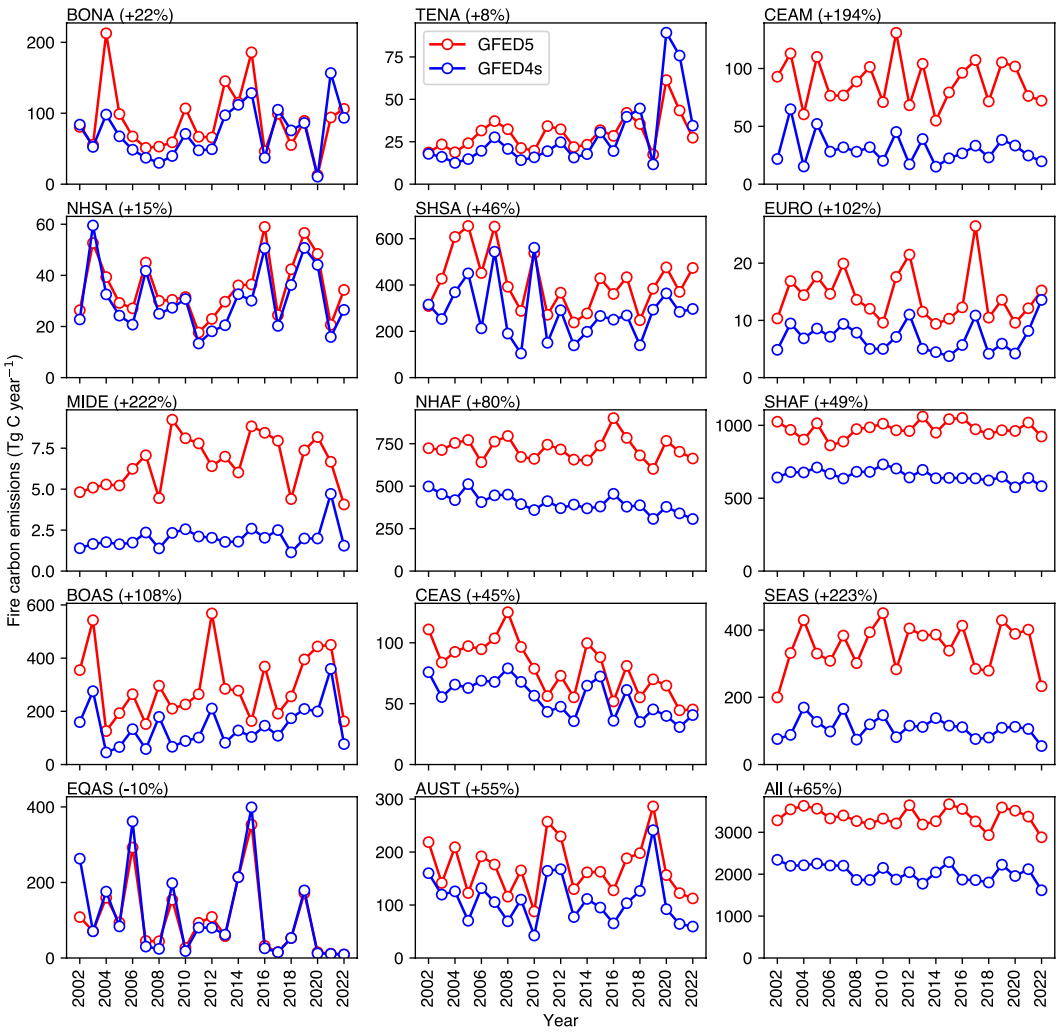

Fig. 5 Annual fire carbon emissions time series for GFED5 and GFED4s for different continental-scale regions defined in Fig. 2 and for the global sum.

different way; these values were based on generalized relationships for $PM_{2.5}$ constituents, specifically assuming PM_1 is $0.8 \times PM_{2.5}$, OA is PM_1 minus BC, and the OA/OC ratio is 1.4 (refs. [58,59]).

In GFED4, gaseous non-methane hydrocarbons (NMHC) emission factors were represented by measured species and assumptions about the emission factors of unmeasured NMHC species. In GFED5, this category has been expanded to include a broader range of gaseous non-methane organic compounds (NMOC gaseous), which can consist of oxygen, nitrogen, and sulfur atoms. Application of advanced instrumentation has significantly expanded emission factor data available for this class in recent years, which better represents the totality of gaseous non-methane emissions. The decrease in the corresponding emission factor values for this class indicates that the assumed mass of unmeasured species used in GFED4 was too high.

Pre-MODIS era. For the pre-MODIS era (1997–2000), we generated the GFED5.1 burned area using Along Track Scanning Radiometer (ATSR[60]) and Tropical Rainfall Measuring Mission Visible and Infrared Scanner (TRMM VIRS[61]) active fire data. The scaling coefficients used to convert active fire detections to burned areas[28] were calibrated against the updated GFED5.1 burned area data. We applied a fuel consumption lookup table to the monthly GFED5.1 burned area to estimate emissions. This lookup table was developed using data from 2002–2011, drawing on GFED5.1 burned area and fire emissions. The table was stratified by 14 GFED regions (Fig. 2) and 16 land cover classes (Table 2), reflecting region- and fire type-specific burning characteristics. This early time range (2002–2011) in the MODIS era was deliberately selected to minimize biases associated with long-term trends in fuel consumption. The fuel consumption values in this lookup table were subsequently used to estimate GFED5 monthly emissions for the pre-MODIS era (1997–2000, at 1° resolution to reflect larger uncertainty) and for 2001 (at 0.25° resolution). Due to the unavailability of land cover stratification for GFED5.1 burned area data in the pre-MODIS era, we assumed that the distribution of burned area across different land cover classes within each 1° grid cell aligns with the monthly climatology from 2002 to 2011 for the burned area-to-emissions conversion. Since data from the 500-m donor study were not available for 2001, we also applied

Species	Savanna and grassland	Boreal forest	Temperate forest	Tropical forest	Peatlands	Agriculture
CO_2	1636[a]	1610	1581	1625	1572	1441
CO	57[a]	114[c]	96	111	225	58
CH_4	1.60[a]	5.04[c]	4.74	4.68	11.10	2.14
NMOC (gaseous)	15.33	15.34	24.31	6.80	36.59	21.40
H_2	1.70	2.03[d]	2.03	3.36	1.22	2.07
NO_x (as NO)	4.00	1.21	1.65	2.55	0.93	2.05
N_2O	0.15[a]	0.21	0.16	0.21[f]	0.21[f]	0.15[g]
PM2.5	5.95	12.77	17.94	9.11	24.78	12.74
TPC	2.99	7.39	10.87	4.33	13.19	9.92
OC	2.62	7.08[e]	10.43	3.99	13.17	9.47
BC	0.37	0.31	0.44	0.34	0.02	0.45
SO_2	0.90	0.56	0.95	0.40	2.06	1.25
C_2H_6	0.66	0.96	0.79	0.71	2.52	0.52
CH_3OH	1.23	2.14	1.83	2.43	3.69	1.69
C_2H_5OH	0.25[b]	0.03	0.18	0.03[f]	0.34	0.25
C_3H_8	0.10	0.31	0.30	0.13	4.06	0.17
C_2H_2	0.25	0.34	0.33	0.44	0.17	0.24
C_2H_4	0.92	1.66	1.36	1.06	1.53	0.89
C_3H_6	0.73	0.83	0.69	0.64	1.86	0.37
C_5H_8	0.08	0.43	0.26	0.13	0.65	0.29
$C_{10}H_{16}$	0.03	3.16	0.90	3.16[f]	0.24	0.06
C_7H_8	0.11	1.54	0.43	0.26	0.78	0.19
C_6H_6	0.22	0.75	0.51	0.39	1.32	0.24
C_8H_{10}	0.02	0.13	0.10	0.13	0.33	0.05
Toluene lump	0.32	2.21	0.95	0.71	2.23	0.44
Higher alkenes	0.10	0.50	0.45	0.21	1.81	0.37
Higher alkanes	0.04	0.23	0.25	0.07	2.17	0.12
CH_2O	1.26	1.68	2.04	1.73	1.35	1.75
C_2H_4O	1.64	1.60	1.56	1.55	1.81	2.10
C_3H_6O	0.42	0.73	0.64	0.63	0.93	0.50
NH_3	0.66	1.47	1.06	1.33	6.15	0.97
C_2H_6S	0.013	0.004	0.016	0.001	0.030	0.014
HCN	0.41	0.93	0.49	0.42	4.68	0.32
HCOOH	0.25	0.45	0.50	0.79	0.41	0.50
CH_3COOH	3.76	3.38	2.51	3.05	5.50	2.65
MEK	0.14	0.10	0.17	0.50	0.26	0.25
CH_3COCHO	0.64	0.48	0.53	0.48[f]	0.19	1.12
$HOCH_2CHO$	0.73	0.74	0.57	2.84	1.52	1.61
Dry matter carbon content (%)	47.2	49.2	47.6	49.4	53.3	41.9

Table 6. Emission factors in grams emitted per kilogram of dry matter burned for six different fire types, based mostly on NEIVA. [a]Dry matter weighted average of spatiotemporally variable emission factors[41]. [b]Based on agriculture values. [c]Average of NEIVA and tower measurements[42]. [d]Based on temperate forest values. [e]Based on PM2.5 and stoichiometry (see text). [f]Based on boreal forest values. [g]Based on savanna values.

the fuel consumption look-up table for emissions estimates for this year, but report the data at 0.25° given the availability of MODIS-derived land cover and burned area.

Daily and hourly fire emissions. Daily fire emissions estimates are often required in atmospheric modeling applications and were used in the dynamic emissions factor model in savannas[41]. To partition monthly carbon emissions from GFED5 to a daily time step at a 0.25° resolution during the MODIS era (2001–2022), we used active fire observations from MODIS collection 6.1 (ref. [48]). Emissions were assumed to be directly proportional to the number of active fire observations on a given day, and several examples are shown in Fig. 6. In rare instances when the MODIS active fire observations were not available, we used active fire observations from SUOMI/VIIRS collection 2 (ref. [62]) or daily burned area fractions from MCD64A1 collection 6.1. For the pre-MODIS era, daily ATSR active fire data[60] were used to distribute emissions, and if daily active fires were not available, we applied a daily climatology (to capture seasonal trends). Because of the much higher uncertainties during the pre-MODIS era, the spatial resolution of the daily fractional emissions product is provided at 1° resolution, matching the resolution of the monthly emissions products during this era.

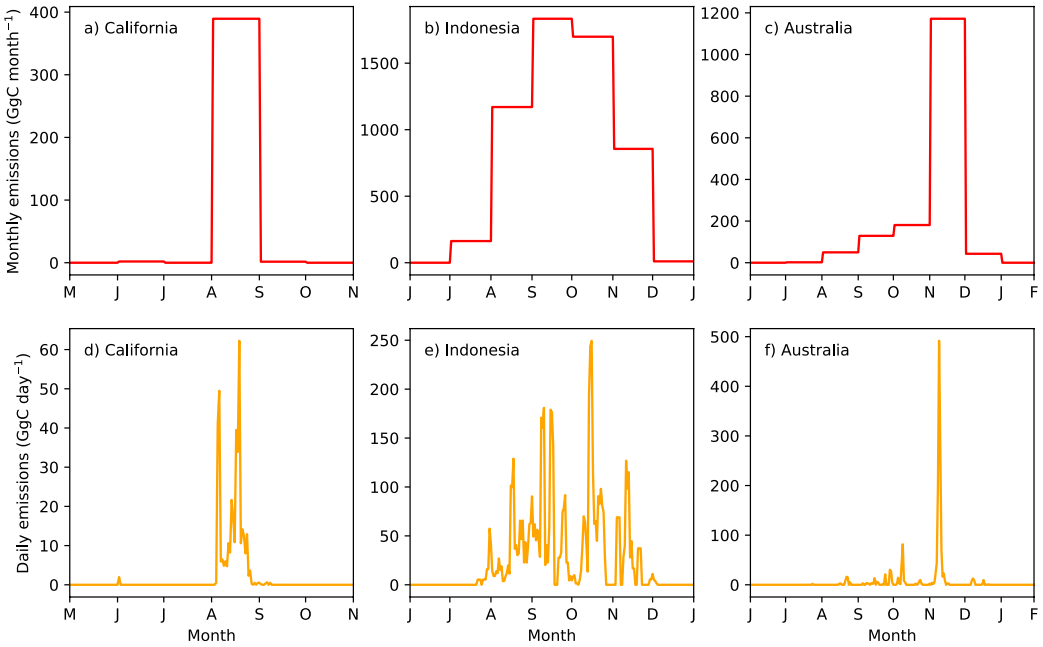

Fig. 6 Monthly and daily GFED5 fire emissions for example 0.25° grid cells. (**a,d**) California in 2021 (40.375°N, 121.375°W), (**b,e**) Indonesia in 2015 (3.375°S, 111.875°E) and (**c,f**) Australia in 2019–2020 (29.875°S, 152.375°E).

We also provide an hourly fire emissions fraction climatology with GFED5. For this product, we used GOES 16 and GOES 17 active fire observations[63] to create mean diurnal cycles for the land cover classes shown in Table 2. GOES 16 and 17 perform a full scan once every 10 minutes, providing six sets of observations per hour. We specifically used moderate and high confidence active fire observations with a view zenith angle less than 75° from North and South America to create the land cover-specific diurnal cycles. In a subsequent step, in each 0.25° grid cell, we then applied weights to each land cover-specific mean diurnal cycle by the amount of annual mean carbon emissions from this class. Diurnal cycles for different land cover classes from boreal, temperate, and tropical ecosystems are shown in Fig. 7.

Data Records

GFED5 data records are available at https://doi.org/10.5281/zenodo.16794692 (ref. [64]). In addition to the repository data, the data records, including newly produced data for more recent years, are also available via https://www.globalfiredata.org. All files are in the NetCDF4 format. The repository contains two sets of files with trace gas emissions, one with a monthly time step and another with a daily time step. Each file contains fire emissions of carbon (C), dry matter (DM), CO_2, CO, CH_4, NMOC_g (where g = gaseous), H_2, NO_x (as NO), N_2O, PM2.5, TPC, OC, BC, SO_2, NH_3, C_2H_6, CH_3OH, C_2H_5OH, C_3H_8, C_2H_2, C_2H_4, C_3H_6, C_5H_8, $C_{10}H_{16}$, C_7H_8, C_6H_6, C_8H_{10}, toluene lump, higher alkenes, higher alkanes, CH_2O, C_2H_4O, C_3H_6O, C_2H_6S, HCN, HCOOH, CH_3COOH, MEK, CH_3COCHO, and $HOCH_2CHO$. In addition, monthly files are available that include burned area and carbon emissions, as well as the partitioning into the 16 land cover classes. These files also contain ancillary layers, including a map of GFED basis regions and the surface area of each grid cell.

Data overview. Annual average global fire carbon emissions according to GFED5 were 3.4 Pg C yr^{-1} during 2002–2022, 65% higher than those from GFED4s. The increases in emissions compared to GFED4s were largest (up to a factor of 3) in fragmented and human-dominated regions, such as Central America, Europe, and Southeast Asia; moderate in savanna ecosystems; and smallest in deforestation-dominated regions. The increase in fire carbon emissions in GFED5, relative to earlier versions of this inventory, propagates through to the emissions of various trace gases and aerosol species. The differences in emission factors between NEIVA and those used in GFED4s are often substantial, sometimes having a larger influence on increases in emissions of individual species than increases in carbon (and dry matter) emissions (Table 7). New emission factors also caused dry matter emissions to increase more (+69%) than carbon emissions, primarily due to the lower CO_2 emission factor for savannas and agricultural burning, which results in lower calculated dry matter carbon content values and thus higher dry matter-to-carbon ratios. On average, lower emission factors than in GFED4 for CO, CH_4, N_2O, and BC dampened the effect of higher dry matter emissions, yielding smaller relative increases compared to GFED4. The opposite was the case for NO_x and SO_2.

Fire emissions vary substantially from year to year and over time. Over the 2002–2022 period, burned area declined[65] with a rate of −1.2% y^{-1}. Carbon emissions, however, only declined with a non-significant −0.3% y^{-1} trend (Fig. 8c). A comparable trend is observed for CO. The declining trend will be even smaller and possibly

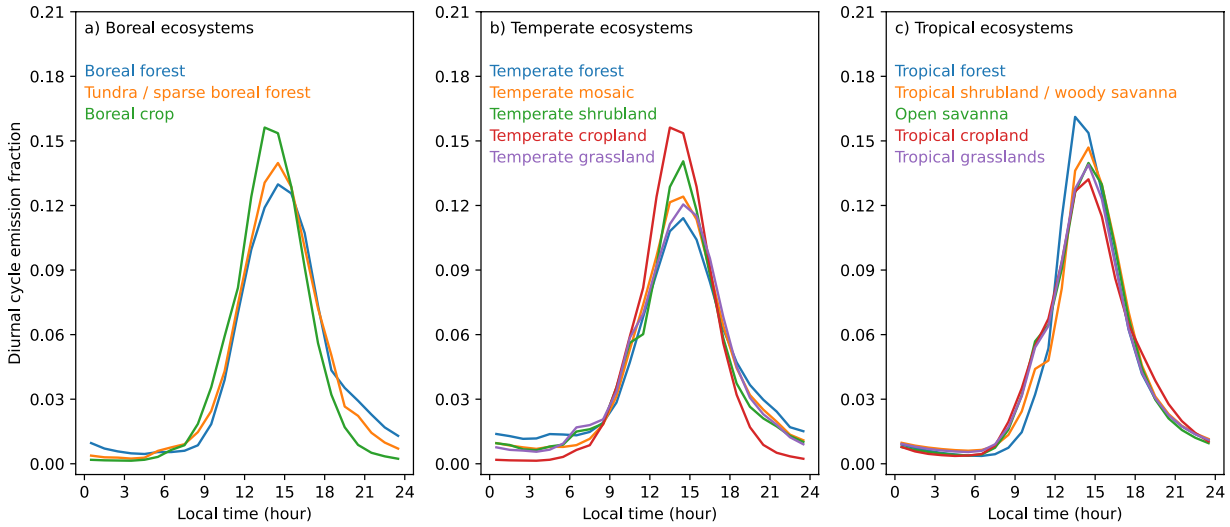

Fig. 7 Diurnal cycles of emission fractions in (**a**) boreal, (**b**) temperate, and (**c**) tropical ecosystems. The hourly fractions for each curve sum to one over 24 hours.

Emissions component	GFED5	GFED4s	Difference (%)
DM (dry matter)	7076	4176	+69
C (total carbon)	3364	2037	+65
CO_2	11476	6902	+66
CO	517	334	+55
CH_4	18.2	14.6	+24
NMOC (gaseous)	110	173	−37
H_2	13.4	8.7	+55
NO_x (as NO)	23.9	13.5	+77
N_2O	1.17	0.89	+31
PM2.5	56.1	35.0	+60
TPC	30.1	17.9	+68
OC	27.6	16.1	+71
BC	2.52	1.77	+43
SO_2	6.16	2.25	+173
NH_3	6.90	4.08	+69

Table 7. Annual emissions for several fire-emitted species for GFED5 and GFED4s (in Tg y^{-1}) and the difference, averaged over 2002–2022.

turn into a positive trend when the high fire years 2023 (ref. [66]) and 2024 are added. The underlying reason for the mismatch in slope strength between burned area and emissions is primarily due to a gradual increase in fuel consumption over time, which offsets part of the decline in burned area. This increase in fuel consumption was partly related to an increasing contribution of forest fires, with relatively high fuel consumption. The increasing fraction of forest emissions also leads to global average emissions of reduced species increasing over time, although the effect is small (Fig. 8c,d). However, fuel consumption also increased in grassland classes (Fig. 8b), partly due to fires moving into higher fuel load areas, as indicated by an increasing trend in fractional tree cover in which fires occurred in all categories except tropical forest fires. The decrease in burned area in GFED5 is slightly smaller than in GFED4s because small fires—captured more effectively in GFED5—have a weaker declining trend than larger fires[28], thus requiring less compensation from increased fuel consumption over time to arrive at relatively constant emissions.

Technical Validation

Both the GFED5 burned area and the fuel consumption data have been constructed to match test observations as closely as possible[28,46]. The data presented here are based on multiplying those two datasets with several modifications. While these estimates represent a significant improvement over previous GFED versions due to advances in all layers necessary for emissions computation, they still carry substantial uncertainty. The actual uncertainty is difficult to quantify, and atmospheric studies providing top-down constraints on our bottom-up estimates are necessary to evaluate the overall magnitude of fire emissions. CO is often used for this goal, as the departure from background concentration is considerable near regional fire complexes and in downwind areas,

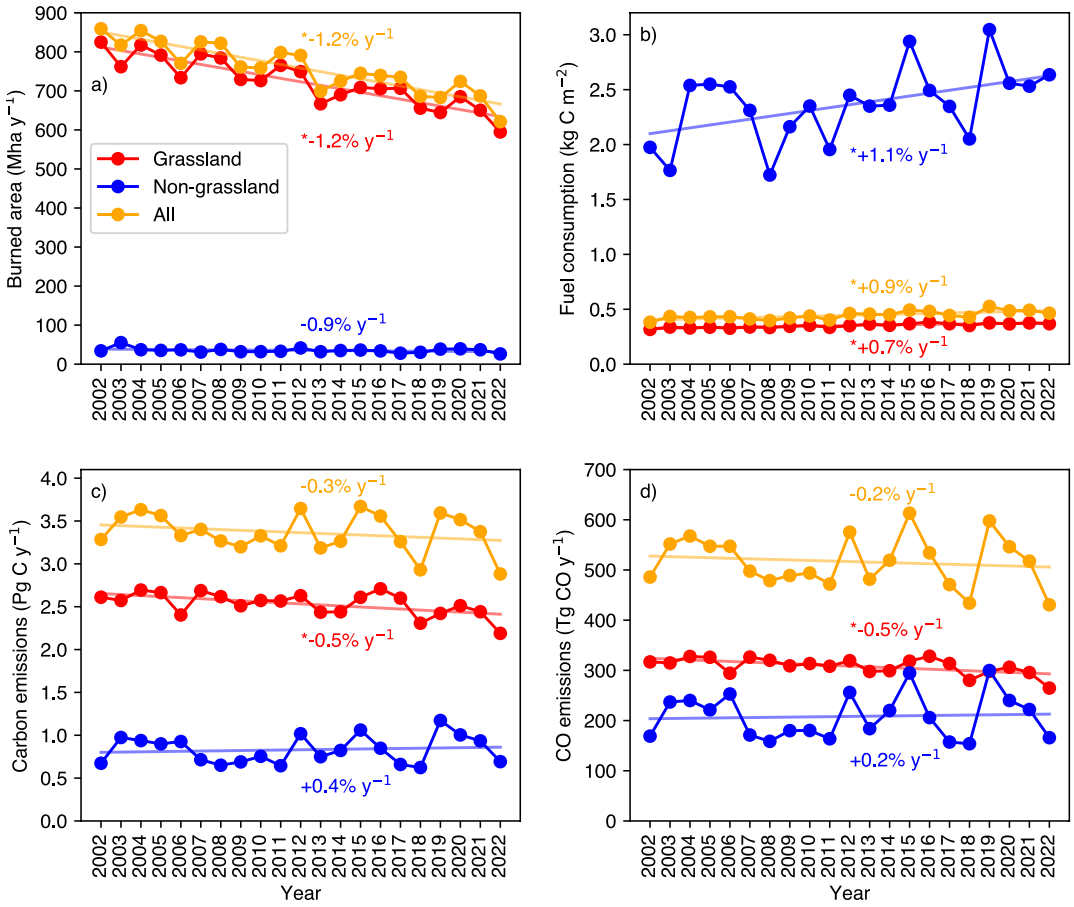

Fig. 8 Mean annual burned area (**a**), fuel consumption (**b**), fire carbon emissions (**c**), and fire carbon monoxide (CO) emissions (**d**) for the 2002–2022 period. The numbers indicate the relative trend, and an asterisk indicates a significant trend ($p < 0.05$).

the chemistry of CO production and oxidation is relatively well understood, and CO can be measured from space.

We leverage previous work using atmospheric CO inversions to estimate fire emissions and compare our new emissions with their results (Table 8). For example, boreal fire emissions have been constrained using carbon monoxide (CO) data from the Measurement of Pollution in the Troposphere (MOPITT) satellite instrument[22], which has also been applied to the 2015 high-fire year in Indonesia[67], to global fire CO emissions in efforts to quantify methane (CH_4) emissions[68], and to fire emissions in the Amazon[69]. We also compared our estimate with those from the 2019–2020 black summer fire event in Southeastern Australia using TROPOspheric Monitoring Instrument (TROPOMI) satellite CO data[70], and the 2019 fire season in southern Africa, also using TROPOMI[71]. This list is not exhaustive, and many other studies have used one of the sensors mentioned above to constrain (fire) emissions (e.g.[72–75]), and many more have used aerosol optical depth (AOD) as a constraint. Studies employing AOD, in general, indicate that previous inventories, including GFED4s were too low[19,76,77], although other factors than underestimated emissions may play a role in explaining the general mismatch between modelled and observed AOD[78].

In the 2021 high boreal fire year, GFED5 estimates are lower than GFED4s and somewhat closer to the top-down constraint[22] (Table 8). While the agreement improved for that year, for earlier years, this is the opposite, and GFED5 then exceeds the top-down estimates. Without the modifications we introduced to downscale fuel consumption in frequently burning regions, GFED5 would have been even higher in this region (+35%).

In southern Africa in 2019, the 46% increase in CO emissions brings GFED5 in closer agreement with the top-down constraint[71], but emissions still seem conservative. It should be noted that the atmospheric analysis using TROPOMI was not a formal inversion where fire emissions, including their spatial and temporal variability, were optimized to best match observations, as in the other studies in Table 8. The top-down estimate of 184 Tg CO shown in Table 8 was derived from the highest bottom-up emission scenario, given that this scenario best matched satellite CO observations after being transported into the atmosphere. Southern Africa is a region where burned areas from small fires are relatively well constrained, fuel consumption has been extensively measured, and CO emission factors are well characterized. The GFED5 underestimation is therefore somewhat surprising, and formal inversions that also optimize for other sources of CO may better pinpoint whether our estimates are indeed still conservative or whether uncertainties in atmospheric studies also explain part of the mismatch.

	Study region	Study period	Top-down estimate	GFED5	GFED4s
Zheng *et al.*[22]	Boreal region	2021	129	122	139
Van der Velde *et al.*[71]	Southern Africa	2019	184	127	87
Van der Velde *et al.*[70]	SE Australia	2019–2020	50	32	27
Yin *et al.*[67]	Indonesia	2015	122	122	110
Naus *et al.*[69]	Amazon	2010–2018	62	59	42
Zhao *et al.*[68]	Global	2002–2021	435	521	338

Table 8. Comparison of CO emission estimates (in Tg CO) from several top-down studies focusing on different fire events with those from GFED5 and GFED4s.

For the Australian Black Summer fires, GFED5 and GFED4s are relatively similar; GFED5 is closer to the top-down constraint[70], although still conservative. One of the few regions where fire carbon emissions decreased in GFED5 compared to GFED4 is equatorial Asia, with Indonesia being responsible for the vast majority of the emissions. Due to an overall higher CO emission factor, the fire CO emissions here are somewhat higher than in GFED4s and close to the top-down constraint in Table 8 (ref. [67]) as well as other studies focusing on the 2015 fires[75,79]. Interestingly, the fire carbon emission estimate for GFED4s is closer to the top-down estimate[67] than GFED5. However, if carbon emission estimates are reported in studies such as those listed in Table 8, they are derived from satellite-constrained CO emission estimates and C-to-CO ratios based on emission factors. Given that these ratios are becoming better constrained, the derived carbon estimate may require further adjustment. The range within the Indonesia-focused top-down studies also shows that uncertainties in top-down constraints are still substantial, for example, due to model setup or the satellite instrument used[79]. For the Amazon, the increase in fire emissions brings GFED5 also close in line with top-down constraints[69].

Finally, our global fire CO estimate now exceeds 500 Tg CO for 2002–2021, a much larger increase compared to the 338 Tg CO in GFED4s than required to match available satellite observations according to a recent global inversion study[68]. That study used GFED4 as a prior, however, and the global total could be higher when using a higher prior such as GFED5. It is interesting to note that reconciling the results from some of the studies listed in Table 8 is not straightforward; the global fire CO estimate[68] for 2019 was 482 Tg CO and for southern Africa, it was 184 Tg CO for that same year[71]. This would mean, according to the atmospheric inversions, that southern Africa is responsible for around 38% of the global total fire emissions, whereas in GFED4s and GFED5, its contribution is considerably smaller, at around 22%. The distribution of MODIS active fire detections (30% in SHAF) and fire radiative power (28% in SHAF) falls between these two values. Now that bottom-up estimates are converging with top-down results, a multi-model and multi-sensor (e.g., MOPITT, TROPOMI) and ideally multi-species (CO, aerosols) intercomparison study is needed to better understand the causes of the remaining uncertainties.

Data availability

GFED5 data records are available at https://doi.org/10.5281/zenodo.16794692 (ref. [64]). In addition to the repository data, the data records including newly produced data for more recent are also available via https://www.globalfiredata.org.

Code availability

The Python (version 3.11) code used to construct GFED5 emissions as well as the various plots and tables can be downloaded from https://doi.org/10.5281/zenodo.16794692 (ref. [64]). The required packages used include Numpy, Matplotlib, Cartopy, netCDF4, and h5py.

Received: 8 April 2025; Accepted: 7 October 2025;
Published online: 28 November 2025

References

1. Glasspool, I. J., Edwards, D. & Axe, L. Charcoal in the Silurian as evidence for the earliest wildfire. *Geology* **32**, https://doi.org/10.1130/G20363.1 (2004).
2. Bowman, D. M. J. S. *et al.* Vegetation fires in the Anthropocene. *Nature Reviews Earth & Environment* **1**, https://doi.org/10.1038/s43017-020-0085-3 (2020).
3. Jones, M. W. *et al.* Global and regional trends and drivers of fire under climate change. *Reviews of Geophysics* **60**, https://doi.org/10.1029/2020RG000726 (2022).
4. Von Danckelman, A. Mémoire sur les Observations Météorologiques faites Sur La Climatologie de la Côte Sud-Ouest D'Afrique en Général. *Association Internationale du Congo* (1884).
5. Crutzen, P., Heidt, L., Krasnec, J., Polluck, W. & Seiler, W. Biomass burning as a source of atmospheric gases CO, H_2, N_2O, NO, CH_3Cl and COS. *Nature* **282**, https://doi.org/10.1038/282253a0 (1979).
6. Seiler, W. & Crutzen, P. J. Estimates of Gross and Net Fluxes of Carbon between the Biosphere and the Atmosphere from Biomass Burning. *Climatic Change* **2**, 207–247 (1980).
7. Crutzen, P. & Andreae, M. Biomass burning in the tropics: Impact on atmospheric chemistry and biogeochemical cycles. *Science* **250**, https://doi.org/10.1126/science.250.4988.1669 (1990).
8. Hoelzemann, J. J., Schultz, M. G., Brasseur, G. P., Granier, C. & Simon, M. Global Wildland Fire Emission Model (GWEM): Evaluating the use of global area burnt satellite data. *Journal of Geophysical Research: Atmospheres* **109**, https://doi.org/10.1029/2003JD003666 (2004).
9. Van der Werf, G. R. *et al.* Continental-Scale Partitioning of Fire Emissions during the 1997 to 2001 El Niño/La Niña Period. *Science* **303**, https://doi.org/10.1126/science.1090753 (2004).

10. Simon, M., Plummer, S., Fierens, F., Hoelzemann, J. J. & Arino, O. Burnt area detection at global scale using ATSR-2: The GLOBSCAR products and their qualification. *Journal of Geophysical Research: Atmospheres* **109**, https://doi.org/10.1029/2003JD003622 (2004).
11. Giglio, L., Boschetti, L., Roy, D. P., Humber, M. L. & Justice, C. O. The Collection 6 MODIS burned area mapping algorithm and product. *Remote Sensing of Environment* **217**, https://doi.org/10.1016/j.rse.2018.08.005 (2018).
12. Lizundia-Loiola, J., Otón, G., Ramo, R. & Chuvieco, E. A spatio-temporal active-fire clustering approach for global burned area mapping at 250 m from MODIS data. *Remote Sensing of Environment* **236**, https://doi.org/10.1016/j.rse.2019.111493 (2020)
13. Van der Werf, G. R. *et al*. Interannual variability in global biomass burning emissions from 1997 to 2004. *Atmospheric Chemistry and Physics* **6**, https://doi.org/10.5194/acp-6-3423-2006 (2006).
14. Van der Werf, G. R. *et al*. Global fire emissions and the contribution of deforestation, savanna, forest, agricultural, and peat fires (1997-2009). *Atmospheric Chemistry and Physics* **10**, https://doi.org/10.5194/acp-10-11707-2010 (2010).
15. Friedlingstein, P. *et al*. Global Carbon Budget 2023. *Earth System Science Data* **15**, 5301–5369, https://doi.org/10.5194/essd-15-5301-2023 (2023).
16. Saunois, M. *et al*. Global Methane Budget 2000-2020. *Earth System Science Data* **17**, 1873–1958, https://doi.org/10.5194/essd-17-1873-2025 (2025).
17. Tian, H. *et al*. Global nitrous oxide budget (1980-2020). Earth System Science. *Data* **16**, 2543–2604, https://doi.org/10.5194/essd-16-2543-2024 (2024).
18. Rabin, S. S. *et al*. The Fire Modeling Intercomparison Project (FireMIP), phase 1: Experimental and analytical protocols with detailed model descriptions. *Geoscientific Model Development* **10**, 1175–1197, https://doi.org/10.5194/gmd-10-1175-2017 (2017).
19. Kaiser, J. W. *et al*. Biomass burning emissions estimated with a global fire assimilation system based on observed fire radiative power. *Biogeosciences* **9**, https://doi.org/10.5194/bg-9-527-2012 (2012).
20. Nabuurs, G.-J. *et al*. Agriculture, Forestry and Other Land Uses (AFOLU). In *Contribution of Working Group III to the Sixth Assessment Report of the Intergovernmental Panel on Climate Change* 747–860 https://doi.org/10.1017/9781009157926.009 (2022).
21. Brown, H. *et al*. Biomass burning aerosols in most climate models are too absorbing. *Nature Communications* **12**, https://doi.org/10.1038/s41467-020-20482-9 (2021).
22. Zheng, B. *et al*. Record-High CO_2 Emissions from Boreal Fires in 2021. *Science* **379**, https://doi.org/10.1126/science.ade0805 (2023).
23. Zhong, Q. *et al*. Threefold Reduction of Modeled Uncertainty in Direct Radiative Effects over Biomass Burning Regions by Constraining Absorbing Aerosols. *Nature Communications* **13**, https://doi.org/10.1126/sciadv.adi3568 (2023).
24. Xu, L. I. *et al*. The Influence of Fire Aerosols on Surface Climate and Gross Primary Production in the Energy Exascale Earth System Model (E3SM). *Journal of Climate* **34**, https://doi.org/10.1175/JCLI-D-21-0193.1 (2021).
25. Randerson, J. T., Chen, Y., van der Werf, G. R., Rogers, B. M. & Morton, D. C. Global burned area and biomass burning emissions from small fires. *Journal of Geophysical Research: Biogeosciences* **117**, https://doi.org/10.1029/2012JG002128 (2012).
26. Van der Werf, G. R. *et al*. Global fire emissions estimates during 1997-2016. *Earth System Science Data* **9**, https://doi.org/10.5194/essd-9-697-2017 (2017).
27. Roteta, E., Bastarrika, A., Padilla, M., Storm, T. & Chuvieco, E. Development of a Sentinel-2 burned area algorithm: Generation of a small fire database for sub-Saharan Africa. *Remote Sensing of Environment* **222**, https://doi.org/10.1016/j.rse.2018.12.011 (2019).
28. Chen, Y. *et al*. Multi-decadal trends and variability in burned area from the fifth version of the Global Fire Emissions Database (GFED5). *Earth System Science Data* **15**, https://doi.org/10.5194/essd-15-5227-2023 (2023).
29. Ramo, R. *et al*. African burned area and fire carbon emissions are strongly impacted by small fires undetected by coarse resolution satellite data. *Proceedings of the National Academy of Sciences of the United States of America* **118**, https://doi.org/10.1073/pnas.2011160118 (2021).
30. Hall, J. V. *et al*. GloCAB: Global cropland burned area from mid-2002 to 2020. *Earth System Science Data* **16**, https://doi.org/10.5194/essd-16-867-2024 (2024).
31. Vallet, L. *et al*. High-resolution data reveal a surge of biomass loss from temperate and Atlantic pine forests, contextualizing the 2022 fire season distinctiveness in France. *Biogeosciences* **20**, https://doi.org/10.5194/bg-20-3803-2023 (2023).
32. Leite, R. V. *et al*. Large scale multi-layer fuel load characterization in tropical savanna using GEDI spaceborne lidar data. *Remote Sensing of Environment* **268**, https://doi.org/10.1016/j.rse.2021.112764 (2022).
33. Eames, T. *et al*. Instantaneous pre-fire biomass and fuel load measurements from multi-spectral UAS mapping in southern African Savannas. *Fire* **4**, https://doi.org/10.3390/fire4010002 (2021).
34. Alonzo, M. *et al*. Patterns of canopy and surface layer consumption in a boreal forest fire from repeat airborne lidar. *Environmental Research Letters* **12**, https://doi.org/10.1088/1748-9326/aa6ade (2017).
35. Walker, X. J. *et al*. Fuel availability not fire weather controls boreal wildfire severity and carbon emissions. *Nature Climate Change* **10**, https://doi.org/10.1038/s41558-020-00920-8 (2020).
36. Russell-Smith, J. *et al*. Opportunities and challenges for savanna burning emissions abatement in southern Africa. *Journal of Environmental Management* **288**, https://doi.org/10.1016/j.jenvman.2021.112414 (2021).
37. Warneke, C. *et al*. Fire Influence on Regional to Global Environments and Air Quality (FIREX-AQ). *Journal of Geophysical Research: Atmospheres* **128**, https://doi.org/10.1029/2022JD037758 (2023).
38. Jayarathne, T. *et al*. Chemical characterization of fine particulate matter emitted by peat fires in Central Kalimantan, Indonesia, during the 2015 El Niño. *Atmospheric Chemistry and Physics* **18**, https://doi.org/10.5194/acp-18-2585-2018 (2018).
39. Wooster, M. J. *et al*. New tropical peatland gas and particulate emissions factors indicate 2015 Indonesian fires released far more particulate matter (but less methane) than current inventories imply. *Remote Sensing* **10**, https://doi.org/10.3390/rs10040495 (2018).
40. van der Velde, R. I. *et al*. Biomass burning combustion efficiency observed from space using measurements of CO and NO_2 by the TROPOspheric Monitoring Instrument (TROPOMI). *Atmospheric Chemistry and Physics* **21**, https://doi.org/10.5194/acp-21-597-2021 (2021).
41. Vernooij, R. *et al*. Dynamic savanna burning emission factors based on satellite data using a machine learning approach. *Earth System Dynamics* **14**, https://doi.org/10.5194/esd-14-1039-2023 (2023).
42. Wiggins, E. B. *et al*. Boreal forest fire CO and CH_4 emission factors derived from tower observations in Alaska during the extreme fire season of 2015. *Atmospheric Chemistry and Physics* **21**, https://doi.org/10.5194/acp-21-8557-2021 (2021).
43. Binte Shahid, S., Lacey, F. G., Wiedinmyer, C., Yokelson, R. J. & Barsanti, K. C. NEIVAv1.0: Next-generation Emissions InVentory expansion of Akagi et al. (2011) version 1.0. *Geoscientific Model Development* **17**, https://doi.org/10.5194/gmd-17-7679-2024 (2024).
44. Akagi, S. K. *et al*. Emission factors for open and domestic biomass burning for use in atmospheric models. *Atmospheric Chemistry and Physics* **11**, https://doi.org/10.5194/acp-11-4039-2011 (2011).
45. Andreae, M. O. Emission of trace gases and aerosols from biomass burning - An updated assessment. *Atmospheric Chemistry and Physics* **19**, https://doi.org/10.5194/acp-19-8523-2019 (2019).
46. van Wees, D. *et al*. Global biomass burning fuel consumption and emissions at 500 m spatial resolution based on the Global Fire Emissions Database (GFED). Geoscientific Model *Development* **15**, https://doi.org/10.5194/gmd-15-8411-2022 (2022).
47. Storey, E. A., Lee West, K. R. & Stow, D. A. Utility and optimization of LANDSAT-derived burned area maps for southern California. *International Journal of Remote Sensing* **42**, https://doi.org/10.1080/01431161.2020.1809741 (2021)
48. Giglio, L., Schroeder, W. & Justice, C. O. The collection 6 MODIS active fire detection algorithm and fire products. *Remote Sensing of Environment* **178**, https://doi.org/10.1016/j.rse.2016.02.054 (2016).
49. Potter, C. S. *et al*. Terrestrial ecosystem production: A process model based on global satellite and surface data. *Global Biogeochemical Cycles* **7**, https://doi.org/10.1029/93GB02725 (1993).

50. Muñoz Sabater, J. ERA5-Land Monthly Averaged Data from 1950 to Present. *Copernicus Climate Change Service (C3S) Climate Data Store (CDS)*, https://doi.org/10.24381/cds.68d2bb30 (2019).
51. Myneni, R., Knyazikhin, Y. & Park, T. MYD15A2H MODIS/Aqua Leaf Area Index/FPAR 8-Day L4 Global 500 m SIN Grid. https://doi.org/10.5067/MODIS/MYD15A2H.006 (2015).
52. DiMiceli, C., Townshend, J., Carroll, M. & Sohlberg, R. Evolution of the representation of global vegetation by vegetation continuous fields. *Remote Sensing of Environment* **254**, https://doi.org/10.1016/j.rse.2020.112271 (2021).
53. Hansen, M. C. *et al*. High-resolution global maps of 21st-century forest cover change. *Science* **342**, https://doi.org/10.1126/science.1244693 (2013).
54. van Leeuwen, T. T. *et al*. Biomass burning fuel consumption rates: A field measurement database. *Biogeosciences* **11**, https://doi.org/10.5194/bg-11-7305-2014 (2014).
55. Van Wees, D. *et al*. Field data synthesis accompanying 'Global biomass burning fuel consumption and emissions at 500-m spatial resolution based on the Global Fire Emissions *Database (GFED)*'. https://doi.org/10.5281/zenodo.6670869 (2022).
56. Travis, K. R. *et al*. Emission Factors for Crop Residue and Prescribed Fires in the Eastern US During FIREX-AQ. *Journal of Geophysical Research: Atmospheres* **128**, https://doi.org/10.1029/2023JD039309 (2023).
57. Desservettaz, M. *et al*. Emission factors of trace gases and particles from tropical savanna fires in Australia. *Journal of Geophysical Research* **122**, https://doi.org/10.1002/2016JD025925 (2017).
58. Reid, J. S., Koppmann, R., Eck, T. F. & Eleuterio, D. P. A Review of Biomass Burning Emissions Part II: Intensive Physical Properties of Biomass Burning Particles. *Atmospheric Chemistry and Physics* **5**, https://doi.org/10.5194/acp-5-799-2005 (2005).
59. Gkatzelis, G. I. *et al*. Parameterizations of US wildfire and prescribed fire emission ratios and emission factors based on FIREX-AQ aircraft measurements. *Atmospheric Chemistry and Physics* **24**, https://doi.org/10.5194/acp-24-929-2024 (2024).
60. Arino, O., Goloub, P., Rosaz, J. M. & Goloup, P. The ATSR World Fire Atlas A synergy with Polder aerosol products. *Proceedings of the International Workshop on the Applications of the ERS Along Track Scanning Radiometer* (1999).
61. Giglio, L., Kendall, J. & Mack, R. A multi-year active fire dataset for the tropics derived from the TRMM VIRS. *International Journal of Remote Sensing* **22**, https://doi.org/10.1080/0143116031000070283 (2003).
62. Schroeder, W., Oliva, P., Giglio, L. & Csiszar, I. A. The New VIIRS 375 m active fire detection data product: Algorithm description and initial assessment. *Remote Sensing of Environment* **143**, https://doi.org/10.1016/j.rse.2013.12.008 (2014).
63. Hall, J. V., Zhang, R., Schroeder, W., Huang, C. & Giglio, L. Validation of GOES-16 ABI and MSG SEVIRI active fire products. *International Journal of Applied Earth Observation and Geoinformation* **83**, https://doi.org/10.1016/j.jag.2019.101928 (2019).
64. Van der Werf, G. *et al*. Global Fire Emissions Database version 5 (GFED5) [Data set]. *Zenodo*, https://doi.org/10.5281/zenodo.16794692.
65. Andela, N. *et al*. A human-driven decline in global burned area. *Science* **356**, https://doi.org/10.1126/science.aal4108 (2017).
66. Byrne, B. *et al*. Carbon emissions from the 2023 Canadian wildfires. *Nature* **633**, https://doi.org/10.1038/s41586-024-07878-z (2024).
67. Yin, Y. *et al*. Variability of fire carbon emissions in equatorial Asia and its nonlinear sensitivity to El Niño. *Geophysical Research Letters* **43**, https://doi.org/10.1002/2016GL070971 (2016).
68. Zhao, J. *et al*. Enhanced CH_4 emissions from global wildfires likely due to undetected small fires. *Nature Communications* **16**, https://doi.org/10.1038/s41467-025-56218-w (2025).
69. Naus, S. *et al*. Sixteen years of MOPITT satellite data strongly constrain Amazon CO fire emissions. *Atmospheric Chemistry and Physics* **22**, https://doi.org/10.5194/acp-22-14735-2022 (2022).
70. van der Velde, I. R. *et al*. Vast CO_2 release from Australian fires in 2019–2020 constrained by satellite. *Nature* **597**, https://doi.org/10.1038/s41586-021-03712-y (2021).
71. van der Velde, I. R. *et al*. Small Fires, Big Impact: Evaluating Fire Emission Estimates in Southern Africa Using New Satellite Imagery of Burned Area and Carbon Monoxide. *Geophysical Research Letters* **51**, https://doi.org/10.1029/2023GL106122 (2024).
72. Griffin, D. *et al*. Biomass burning CO emissions: exploring insights through TROPOMI-derived emissions and emission coefficients. *Atmospheric Chemistry and Physics* **24**, https://doi.org/10.5194/acp-24-10159-2024 (2024).
73. Nguyen, H. M., He, J. & Wooster, M. J. Biomass burning CO, PM and fuel consumption per unit burned area estimates derived across Africa using geostationary SEVIRI fire radiative power and Sentinel-5P CO data. *Atmospheric Chemistry and Physics* **23**, https://doi.org/10.5194/acp-23-2089-2023 (2023).
74. Peiro, H., Crowell, S. & Moore, B. Optimizing 4 years of CO_2 biospheric fluxes from OCO-2 and *in situ* data in TM5: fire emissions from GFED and inferred from MOPITT CO data. *Atmospheric Chemistry and Physics* **22**, https://doi.org/10.5194/acp-22-15817-2022 (2022).
75. Huijnen, V. *et al*. Fire carbon emissions over maritime southeast Asia in 2015 largest since 1997. *Scientific Reports* **6**, https://doi.org/10.1038/srep26886 (2016).
76. Mallet, M. *et al*. Climate Models Generally Underrepresent the Warming by Central Africa Biomass-Burning Aerosols over the Southeast Atlantic. *Science Advances* **7**, https://doi.org/10.1126/sciadv.abg9998 (2021).
77. Reddington, C. L. *et al*. Analysis of particulate emissions from tropical biomass burning using a global aerosol model and long-term surface observations. *Atmospheric Chemistry and Physics* **16**, https://doi.org/10.5194/acp-16-11083-2016 (2016).
78. Zhong, Q. *et al*. Using modelled relationships and satellite observations to attribute modelled aerosol biases over biomass burning regions. *Nature Communications* **13**, https://doi.org/10.1038/s41467-022-33680-4 (2022).
79. Nechita-Banda, N. *et al*. Monitoring emissions from the 2015 Indonesian fires using CO satellite data. *Philosophical Transactions of the Royal Society* **373**, https://doi.org/10.1098/rstb.2017.0307 (2018).
80. Sulla-Menashe, D., Gray, J. M., Abercrombie, S. P. & Friedl, M. A. Hierarchical mapping of annual global land cover 2001 to present: The MODIS Collection 6 Land Cover product. *Remote Sensing of Environment* **222**, https://doi.org/10.1016/j.rse.2018.12.013 (2019).

Acknowledgements

We thank Bo Zheng for sharing inversion results and for helpful discussion, and Elena Kukavskaya and Sander Veraverbeke for discussing fuel consumption dynamics in the boreal region. This research has been funded by the Netherlands Organization for Scientific Research (VICI research program 016.160.324), the CALIPSO project, funded through the generosity of Eric and Wendy Schmidt by recommendation of the Schmidt Futures program, and NOAA Global Monitoring Laboratory. J. Randerson, Y. Chen, and D. Morton acknowledge funding support from NASA's Modelling, Analysis, and Prediction (80NSSC21K1362), Earth Information System-Fire (EIS-Fire), Interdisciplinary Science (80NSSC24K0301), and FireSense (80NSSC24K1317, 80NSSC25K0393) programs. J. Randerson acknowledges additional funding support from NASA (80NSSC25K7211), the U.S. National Science Foundation (RISE-2425932), and the U.S. Dept. of Energy Office of Science Biological and Environmental Research RUBISCO Science Focus Area. R. Yokelson acknowledges funding support from the U.S. National Science Foundation Atmospheric Chemistry Program grants AGS-1748266 and AGS-1349976, NOAA-CPO grant NA16OAR4310100, and NASA grant NNX14AP45G.

Author contributions

G.W.: Conceptualization, modeling development, overall data compilation, analysis, writing. J.R.: Conceptualization, burned area, and daily/hourly fire product development, writing. D.W.: Fuel consumption modeling and emissions data compilation, writing. Y.C.: Burned area product development, writing. L.G.: Burned area product development, editing. J.H.: Cropland burned area product development, editing. R.V.: Savanna emission factor estimation and synthesis, editing. M.M.: Daily/hourly fire product development, editing. S.S.: Emission factor database development. K.B.: Emission factor database development, editing. R.Y.: Emission factor database development, editing. D.M.: Writing.

Competing interests

The authors declare no competing interests.

Additional information

Correspondence and requests for materials should be addressed to G.W.

Reprints and permissions information is available at www.nature.com/reprints.

Publisher's note Springer Nature remains neutral with regard to jurisdictional claims in published maps and institutional affiliations.